Theoretical Study of the Insertion Reactions of Aluminum with H_2O, NH_3, HCl, and Cl_2

Torbjörn Fängström,[†] Sten Lunell,*[,†] Paul H. Kasai,[‡] and Leif A. Eriksson[§]

Department of Quantum Chemistry, Uppsala University, Box 518, S-751 20 Uppsala, Sweden, IBM Research Division, Almaden Research Center, 650 Harry Road, San Jose, California, and Department of Physics, Stockholm University, Box 6730, S-113 85 Stockholm, Sweden

Received: September 3, 1997; In Final Form: November 17, 1997

Stationary points on the potential energy surfaces describing the reactions between Al and H_2O, NH_3, HCl, and Cl_2 respectively, have been optimized at the ab initio MP2 and QCISD levels as well as by density functional theory (DFT) using the B3LYP functional and the 6-31G(d,p) basis set. Reaction energies were computed using the MP2 and B3LYP methods and the QCISD and CCSD(T) methods in conjunction with the 6-311+G(2df,p) and 6-31G(d,p) bases, respectively. Isotropic hyperfine coupling constants (hfcc's) of Al, N, Cl, and H were computed using the MP2, B3LYP, and QCISD methods in conjunction with the 6-311+G(2df,p) basis, and at the PWP86/IGLO-III level for isotropic and anisotropic coupling constants. For HAlCl and $AlCl_2$, the theoretical study predicts positive isotropic Cl hyperfine coupling constants at variance with the previously reported experimental values. A revised analysis of the experimental ESR spectra led to new assignments of the Cl hyperfine coupling tensors, in agreement with the computed results.

I. Introduction

Experimental electron spin resonance (ESR) investigations of reactions between aluminum atoms and small molecules, as well as a number of theoretical studies on the above-mentioned reactions and/or its products, have recently been reported. Examples of the theoretical work include Sakai's investigation of the aluminum insertion mechanism into H_2O, HCl, and NH_3 using Hartree−Fock and Møller−Plesset perturbation theory to second order (MP2) for the geometries and to fourth order (MP4) for the energies[1,2] and Cramer's study of several organic and inorganic radicals containing aluminum.[3] Of relevance for the present work are the structural and hyperfine coupling constant (hfcc) calculations for the AlH(OH) molecule at the MP2 level of theory. A theoretical part was also included in the ESR investigations on the aluminum + water reaction by Joly et al.[4] and Knight et al.[5] and on the aluminum + hydrogen chloride reaction by Köppe and Kasai.[6]

To our knowledge no theoretical calculations have so far been performed for the products of the reactions between aluminum and any of H_2O, NH_3, HCl, or Cl_2, employing the novel density functional theory (DFT) or the quadratic configuration interaction (QCISD) methods. No comparison between theoretical and experimental ESR data has so far been carried through for the products of the reaction between aluminum and NH_3, HCl, or Cl_2. In the present work, parts of the theoretical study by Sakai[1,2] are extended through a more thorough investigation of the potential energy surfaces (PES) governing the reactions between Al and H_2O or NH_3, including more accurate levels of theory and comparisons between experimental and theoretical hfcc's (isotropic and anisotropic). In addition to the investigation of the Al + HCl products, Köppe and Kasai also looked at the Al + Cl_2 reaction.[6] Inspired by this work, the structure and hfcc of the Al insertion product for the Al + Cl_2 reaction have also been determined.

[†] Uppsala University.
[‡] Almaden Research Center.
[§] Stockholm University.

II. Methods

A. Geometries. Full geometry optimizations were performed at the correlated ab initio and hybrid density functional theory levels. In all these calculations the program systems Gaussian-92[7] and Gaussian-94[8] were used. In the ab initio calculations, electron correlation was included through Møller−Plesset perturbation theory[9] to second order (MP2) and through configuration interaction employing the QCISD method.[10] For all geometry optimizations at the MP2 or QCISD levels, the frozen core approximation was used. The functional used in the DFT calculations, referred to as B3LYP, is based on Becke's three-parameter adiabatic connection method (ACM) approach and consists of a combination of Slater,[11] Hartree−Fock,[12] and Becke[13] exchange and the Vosko, Wilk, and Nusair (VWN) local[14] and Lee, Yang, and Parr (LYP)[15] nonlocal correlation functionals. The split valence 6-31G(d,p)[16,17] basis set was used in all ab initio and DFT optimizations.

B. Energies. To obtain more reliable values of the energies at the different stationary points on the potential energy surface (PES), a number of single-poinit calculations were performed using larger basis sets or different methods. For the stationary points on the MP2 or B3LYP PES obtained using the 6-31G(d,p) basis set, single-point calculations were performed at the corresponding level of theory, using the larger 6-311+G(2df,p) basis.[18−22] For the stationary points on the QCISD PES single-point calculations were performed using the coupled-cluster approximation including single and double excitations, with noniterative inclusion of triple excitations, (CCSD(T)).[23] These energies are compared with the energetics from the corresponding QCISD calculations. For the open-shell systems, also the spin-projected MP2 energies, PMP2, are reported, that is, the energies obtained when the first contaminating spin state is annihilated. In the present study this corresponds to annihilating the quartet component of the unrestricted MP2 wave function. The notation (P)MP2 refers to both PMP2 and MP2 values.

C. Hyperfine Coupling Constants. Magnetic interactions between the nuclear spin ($\vec{I}$) and the electronic magnetic

S1089-5639(97)02859-4 CCC: $15.00
Published on Web 01/16/1998

moments, caused by the electron spin ($\vec{S}$), give rise to hyperfine splittings in molecular ESR spectra. The splittings can be divided into an isotropic and an anisotropic part, where the isotropic part is given by a contact interaction (Fermi contact) term[24,25] in the spin Hamiltonian:

$$H_{\text{spin}}^{(1)} = A_N^{(\text{iso})}(\vec{I}\cdot\vec{S}) \tag{1}$$

For a particular nucleus N (assuming a doublet radical) $A_N^{(\text{iso})}$ is

$$A_N^{(\text{iso})} = \frac{8\pi}{3} g\beta_N\beta_N\rho^{(\alpha-\beta)}(\vec{r}_N) \tag{2}$$

Where $\rho^{(\alpha-\beta)}(\vec{r}_N)$ is the spin density at the position of the particular nucleus N. The anisotropic part originates from the dipole−dipole interaction. Again assuming a doublet radical, the corresponding Hamiltonian is given by

$$H_{\text{dipolar}} = g\beta g_N\beta_N\left[\frac{\vec{S}\cdot\vec{I}}{r^3} - \frac{3(\vec{S}\cdot\vec{r})(\vec{I}\cdot\vec{r})}{r^5}\right] \tag{3}$$

Expanding the vectors, we obtain

$$H_{\text{dipolar}} = g\beta g_N\beta_N\left[\left\langle\frac{r^2-3x^2}{r^5}\right\rangle\vec{S}_x\vec{I}_x + \left\langle\frac{r^2-3y^2}{r^5}\right\rangle\vec{S}_y\vec{I}_y + \left\langle\frac{r^2-3z^2}{r^5}\right\rangle\vec{S}_z\vec{I}_z - \left\langle\frac{3xy}{r^5}\right\rangle(\vec{S}_x\vec{I}_y + \vec{S}_y\vec{I}_x) - \left\langle\frac{3xz}{r^5}\right\rangle(\vec{S}_x\vec{I}_z + \vec{S}_z\vec{I}_x) - \left\langle\frac{3yz}{r^5}\right\rangle(\vec{S}_y\vec{I}_z + \vec{S}_z\vec{I}_y)\right] \tag{4}$$

where the brackets imply an integration over spatial coordinates. Introducing the matrix **T**,

$$\mathbf{T} = (-g\beta g_N\beta_N)\begin{bmatrix}\left\langle\frac{r^2-3x^2}{r^5}\right\rangle & -\left\langle\frac{3xy}{r^5}\right\rangle & -\left\langle\frac{3xz}{r^5}\right\rangle\\ \left\langle\frac{3xy}{r^5}\right\rangle & \left\langle\frac{r^2-3y^2}{r^5}\right\rangle & -\left\langle\frac{3yz}{r^5}\right\rangle\\ -\left\langle\frac{3xz}{r^5}\right\rangle & -\left\langle\frac{3yz}{r^5}\right\rangle & \left\langle\frac{r^2-3z^2}{r^5}\right\rangle\end{bmatrix} \tag{5}$$

the dipole−dipole part of the spin Hamiltonian can be written as

$$H_{\text{spin}}^{(2)} = [S_x,S_y,S_z]\cdot\mathbf{T}\begin{bmatrix}I_x\\ I_y\\ I_z\end{bmatrix} \tag{6}$$

Finally introducing the hyperfine tensor **A** in which both the isotropic (fermi contact) and anisotropic (dipole−dipole) parts are included, we have

$$\mathbf{A} = A_N^{(\text{iso})}\mathbf{1} + \mathbf{T} \tag{7}$$

where **1** is the unit matrix.

The hyperfine tensor can be obtained in a diagonal form by rotation of the coordinate system. The coordinate axis which brings the hyperfine tensor into diagonal form is referred to as the principal axis of the tensor.

The isotropic part can again be obtained as the trace of the diagonalized hyperfine tensor,

$$A_N^{(\text{iso})} = \frac{1}{3}\,\text{tr}\,\mathbf{A} \tag{8}$$

The anisotropic part, **T**, of the diagonalized hyperfine tensor, referred to as T_{xx}, T_{yy}, and T_{zz}, respectively, will sum up to zero.

The isotropic hyperfine coupling constants (hfcc's) are thus related to the spin density at a particular nucleus, and the anisotropic couplings are related to the extension of the spin density around a specific nucleus, both of which can be acquired from a calculated wave function. Hence, comparison with measured hyperfine splittings give a good indication of the quality of the calculated wave function and the ability of the method in question to accurately describe the system under study.

We here report hfcc's, isotropic and anisotropic, for those points on the potential energy surface believed to represent possible reaction products. Results are presented for the isotropic hfcc from the MP2, B3LYP, and QCISD calculations using the 6-311+G(2df,p) basis. In the ab initio calculations all electrons were included in the correlation treatment. Isotropic and anisotropic hfcc's were also calculated using the PWP86 function[26−28] and the IGLO-III[29] basis set as implemented in the deMon[30−33] program.

D. Spectral Simulations. Computer programs that simulate an ESR spectrum exhibited by an ensemble of randomly oriented radicals ($S = {}^1/_2$) have been described earlier.[34−36] Briefly recounted, the powder pattern is given by

$$S(H) = \sum_{\text{hfcc}}\int_0^{2\pi}\int_0^{\pi} T_{\text{hfcc}}(\Theta,\varphi)D[H - H_{\text{hfcc}}(\Theta,\varphi)]\sin\Theta\,\mathrm{d}\Theta\,\mathrm{d}\varphi \cong \sum_{\text{hfcc}}\sum_{\Theta}\sum_{\varphi} T_{\text{hfcc}}(\Theta,\varphi)D[H - H_{\text{hfcc}}(\Theta,\varphi)]\sin\Theta\,\Delta\Theta\,\Delta\varphi \tag{9}$$

The angles Θ and φ define the direction of the external magnetic field H relative to the principal g tensor, and the summation over hfcc is performed over all the hyperfine components. Depending on the nuclei and the hfcc tensors, it may also be necessary to include the forbidden transitions arising from the anisotropy of the hfc tensor ($\Delta M_I = \pm1$)[35] and/or the nuclear quadrupole moment ($\Delta M_I = \pm1,\pm2$).[36] $H_{\text{hfcc}}(\Theta,\varphi)$ and $T_{\text{hfcc}}(\Theta,\varphi)$ represent, respectively, the resonance field and the transition probability of the particular hfcc component. $D[H - H_{\text{hfcc}}(\Theta,\varphi)]$ is the derivative of a line shape function and that of a Lorentzian or Gaussian form is used.

In the program, the double integral is approximated by the double-loop summation, as indicated above, where the increment $\Delta\varphi$ for the inner loop is proportionate to 1/sin Θ. Typically summation of signals corresponding to 1000 directions (of the external field) uniformly distributed in the semispherical space is sufficient to produce a smooth powder pattern. When the principal axes of a hyperfine coupling tensor do not coincide with those of the g tensor, the directional cosines of the applied field relative to the hyperfine coupling tensor are given by the directional cosines of the field relative to the g tensor and the Eulerian angles relating the orientation of the hyperfine coupling tensor to that of the g tensor.

III. Results

A. Al + H_2O. Several recent theoretical studies have been performed on the reaction between aluminum atoms and water and/or possible products of the reaction. A first estimate of the stability and the insertion barrier is found in the work by Kurtz and Jordan.[37] In a more thorough work, Sakai employed the MP2 method, in which he found structures of a nonplanar addition complex, a transition state, and a trans H−Al−OH insertion product.[1,2] The reaction was found to be exothermic,

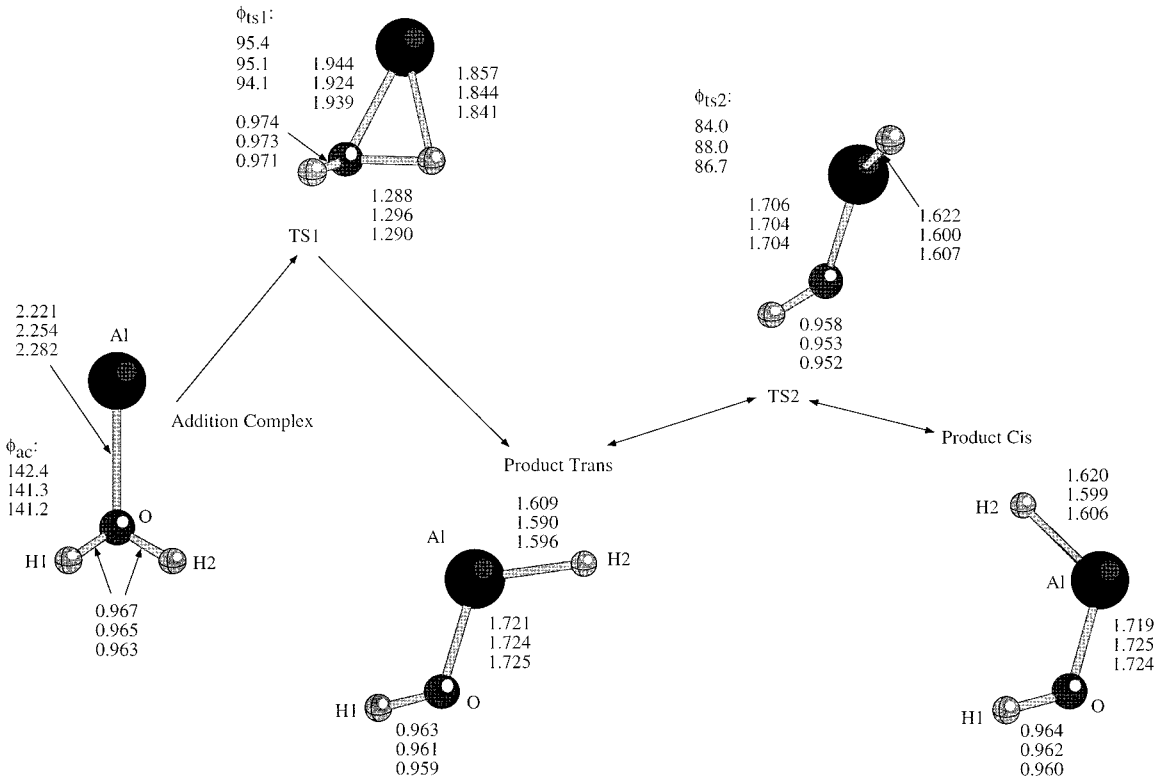

Figure 1. Optimized geometries corresponding to different stationary points on the Al + H_2O potential energy surface. The interatomic distances and angles indicated are obtained, starting from the top, from B3LYP, MP2, and QCISD calculations, respectively. The torsion angles ϕ for the addition complex, TS1, and TS2 are defined as the angles between the planes: H1−O−Al and Al−O−H2 (AC), H1−O−Al and O−Al−H2 (TS1), and H1−O−Al and O−Al−H2 (TS2), respectively.

with the addition complex located about 8 kcal/mol and the insertion product 40 kcal/mol below the reactants in energy, respectively. The energy barrier to the insertion product was reported to be on the order of 16−20 kcal/mol. Knight et al. have in a joint theoretical and experimental work[5] found two planar product structures, one cis and one trans, also using the MP2 method. In the latter study the best agreement between experimental and calculated isotropic and anisotropic hyperfine parameters (employing configuration interaction in the calculations of the hyperfine parameters) was found for the trans structure. Cramer reported calculated isotropic hfcc for the trans structure employing the unrestricted Hartree−Fock method for the geometries and MP2 for the isotropic hfcc.[3] In the work by Joly et al. a procedure similar to the one used by Knight was applied to the Al + H_2O system.[4] Their calculations supported the findings of Knight and of Cramer suggesting the trans structure to be the final product. Due to the small energy difference between the cis and trans conformers and the rather large deviation between experimental and theoretical hfcc found for both structures, the cis structure was however not ruled out as a possible product. Sakai and Jordan suggested finally that the lowest energy path for the cis−trans isomerization will involve an in-plane motion for the hydroxy proton rather than a rotation about the Al−O bond.[38]

1. Geometry Optimizations. One addition complex (AC), two products, one cis and one trans conformer, and two transition states were found at all levels employed in the geometry optimizations MP2/6-31G(d,p), QCISD/6-31G(d,p) and B3LYP/6-31G(d,p), Figure 1. The nonplanar addition complex with C_s symmetry shows a large method dependency in the Al−O distance, which varies between 2.22 Å (B3LYP) and 2.28 Å (QCISD). Except for the Al−O distance in the addition complex, the geometrical parameters at all other stationary points are nearly independent of the choice of method. Both products, cis and trans, are found to be planar by all methods presently used.

Two different transition states were found: one that connects the addition complex with the trans product (TS1) and one that connects the trans product with the cis product (TS2). In TS1 the interaction between the water molecule and the Al atom elongates one of the O−H bonds and shortens the Al−H and Al−O distances compared to the addition complex. The main difference between TS2 and the cis and trans products is the angle between the H1−O−Al and O−Al−H2 planes, which implies the rotation around the Al−O bond to be the reaction coordinate for the cis−trans isomerization. Several attempts were made to localize a planar transition state as suggested by Sakai and Jordan.[38] The planar structures, however, turned out to exhibit two imaginary frequencies, one of which corresponding to an out-of-plane motion. The products and the transition states observed in the present work were verified to be true energy minima or saddle points to first order, respectively, in frequency calculations performed at the MP2/6-31G(d,p) and B3LYP/6-31G(d,p) levels.

To verify the relevance of the transition states found, intrinsic reaction coordinate IRC[39,40] calculations were performed starting from the transition states. Due to the close similarity in geometric structures between the different methods, IRC calculations were performed at the MP2/6-31G(d,p) level only. The points connected via TS1 were confirmed to be the addition complex and the trans product, and the points connected via TS2 were the trans and cis products.

2. Potential Energy Surface. The relative energies of the stationary points optimized at the different levels of approximation are listed in Table 1. The relative stability of the addition complex is rather similar at all levels of theory, 8.7 kcal/mol

TABLE 1: Energies for the Addition Complex, Transition States, and Products of the Al + H_2O Reaction at the MP2/6-311+G(2df,p)//MP2/6-31G(d,p),[a] B3LYP/6-311+G(2df,p)//B3LYP/6-31G(d,p),[b] QCISD/6-31G(d,p),[c] and CCSD(T)/6-31G(d,p)//QCISD/6-31G(d,p)[d] Levels. Energies Are Given in kcal/mol Relative to the Reactants Al and H_2O

	addition complex	transition state I	trans product	transition state II	cis product
MP2	−7.9	9.0	−47.7	−44.6	−46.9
MP2, corr.[e]	−4.5	8.2	−46.4	−44.2	−45.8
PMP2	−8.3	7.0	−47.2	−44.2	−46.3
PMP2, corr.[e]	−4.8	6.3	−45.9	−43.8	−45.2
B3LYP	−6.8	5.8	−44.2	−41.3	−43.0
B3LYP, corr.[e]	−4.9	2.9	−45.1	−43.1	−44.2
QCISD	−8.7	13.1	−38.3	−34.1	−37.1
CCSD(T)	−9.3	11.5	−38.9	−34.5	−37.6

[a] Absolute energies of the reactants (au): MP2, −318.373081; PMP2, −318.374550. [b] Absolute energies of the reactants (au): B3LYP, −318.846912. [c] Absolute energies of the reactants (au): QCISD, −318.129834. [d] Absolute energies of the reactants (au): CCSD(T), −318.132948. [e] The values are corrected for BSSE employing the 6-311+G(2df,p) basis and ZPE employing the 6-31G(d,p) basis; see text.

below the reactants at the QCISD/6-31G(d,p) level and 6.8 kcal/mol at the B3LYP/6-311+G(2df,p)//B3LYP/6-31G(d,p) level, respectively (cf. Table 1). Passing over the first transition state (TS1), in which one of the O−H bonds is elongated, to a trans Al insertion product gives a barrier of 12.6 kcal/mol at the B3LYP level and a considerably larger barrier of 15.3−21.8 kcal/mol at the (P)MP2, QCISD, and CCSD(T) levels (Table 1). As in the case of the addition complex the trans product is most stable at the B3LYP level, 44.2 kcal/mol below the reactants, and least stable at the QCISD/6-31G(d,p) level (38.3 kcal/mol). The trans product is connected to the cis conformer passing over the second transition state (TS2) with a small barrier of 2.9−4.2 kcal/mol, with only minor dependency upon computational method. The calculated stabilities for the two product structures are very similar, with the trans structure being slightly more stable, by 0.8−1.3 kcal/mol.

To check the effects of basis set superposition errors (BSSEs), the counterpoise correction method[41] was applied to TS1 and to the addition complex. Also for TS2 and the product structures, corrections to the BSSE were estimated, this time using Al−H and O−H as reactants. The corrections were calculated at the (P)MP2 and B3LYP levels of approximation using the larger 6-311+G(2df,p) basis set. All stationary points were destabilized 2.4−3.3 kcal/mol at the (P)MP2 levels and a few kilocalories less, around 1 kcal/mol at the B3LYP level (cf. Table 1).

Zero-point vibrational energy corrections (ZPEs) were also calculated for all stationary points at the MP2/6-31G(d,p) and B3LYP/6-31G(d,p) levels. The correction stabilized the transition states and product structures by 1.5−4.0 kcal/mol and destabilized the addition complex about 1 kcal/mol at both computational levels. Including both the ZPE and BSSE corrections destabilizes all minima by 0.4−3.5 kcal/mol, except TS1, which is stabilized by 0.7−0.8 kcal/mol. The insertion barrier is now 12.7 kcal/mol at the MP2 and 11.1 kcal/mol at the PMP2 level. The values for the insertion barrier calculated in the present paper are somewhat lower compared to the ones reported by Sakai (16.4 kcal/mol at the MP2/6-31G(d) level).[2] Those differences in the calculated energy barriers are probably due to the lack of inclusion of BSSE corrections in the work by Sakai, considering that the uncorrected energy barriers at the QCISD, CCSD(T), and MP2 levels in the present paper agree well with the barriers previously reported by Sakai. The cis−trans barrier is at the BSSE and ZPE corrected (P)MP2 levels reduced to 2.2 kcal/mol (MP2) and 2.1 kcal/mol (PMP2). At the B3LYP level the corrections destabilize the stationary points by 0.9−2.9 kcal/mol, and the two barriers are now 7.8 kcal/mol (TS1) and 2 kcal/mol (TS2), respectively (cf. Table 1).

TABLE 2: Isotropic hfcc (G) for the Addition Complex and Product of the Al + H_2O System. The Coupling Constants Are Calculated at the MP2/6-311+G(2df,p)//MP2/6-31G(d,p), B3LYP/6-311+G(2df,p)//B3LYP/6-31G(d,p), PWP86/IGLO-III//QCISD/6-31G(d,p), and QCISD/6-311+G(2df,p)//QCISD/6-31G(d,p)[a] Levels of Theory. Included Are the Calculated Values for the Trans Structure Taken from the Work by Knight et al.,[5] Joly et al.,[4] and Cramer[3]

	structure	A1	H1	H2
MP2	addition complex	−34.7	2.6	2.6
	product cis	368.9	8.0	82.5
	product trans	314.5	−0.7	81.4
B3LYP	addition complex	−15.9	3.3	3.3
	product cis	371.1	10.6	104.5
	product trans	307.9	−1.3	102.2
PWP86	product cis	374.2	11.4	108.3
	product trans	313.5	−1.4	103.7
QCISD	addition complex	−13.2	2.5	2.5
	product cis	362.6	8.3	88.5
	product trans	308.8	−1.2	87.0
exptl[b]		327.2	<2	102.8
Knight[c]	product trans	310.8	−0.7	67.1
Joly[d]	product trans	302.2	−0.7	66.0
Cramer[e]	product trans	300.9	−1.2	82.4

[a] The hfcc's for the addition complex are calculated employing the 6-31G(d,p) basis. [b] Experimental values from the work by Knight et al.[5] [c] Calculated values from ref 5 (geometries optimized at the MP2/6-31G(d,p) level and hfcc calculated employing CISD in conjunction with a double-zeta basis). [d] Calculated values from ref 4 (geometries optimized at the UHF/6-311G(d,p) level and hfcc calculated employing CISD in conjunction with a double-zeta basis). [e] Calculated values from ref 3 (geometries optimized at the UHF/6-31G(d) level and hfcc calculated at the MP2/6-311G(d,p) level).

Comparing the MP2 and PMP2 levels, only small differences in energies are seen for all stationary points except for TS1. This close similarity between the MP2 and PMP2 levels is also seen in the small deviation of $\langle S^2 \rangle$ from the ideal value of 0.75. $\langle S^2 \rangle$ is at most 0.78 except for the transition state, for which a somewhat larger value of 0.83 is found. The values of $\langle S^2 \rangle$ are very similar at the QCISD and MP2 levels, while the deviation from the ideal value is the smallest at the B3LYP level, with a maximum value for $\langle S^2 \rangle$ of 0.76 for TS1.

3. Hyperfine Coupling Constants. The isotropic hyperfine coupling constants (hfcc's) were calculated for the hydrogen atoms and the aluminum atom of the addition complex and the products at the B3LYP, MP2, and QCISD levels, employing the 6-311+G(2df,p) basis set (for the addition complex at the QCISD level, only the smaller 6-31G(d,p) basis was employed) and at the PWP86/IGLO-III level. Reasonable agreement between experimental and calculated values is seen for all methods and both product structures (cis and trans) for the H2 proton and Al, although the calculated Al value for the cis product is too high compared to the experimental value at all levels (cf. Table 2). Excellent agreement between experimental and calculated values is seen for H2 for both products, the maximum deviation being not more than 2.5% at the B3LYP level. The calculated values for H1 in the cis structure are 8−11 G too large compared with the experimental value, irrespective of the method used. The observed discrepancy between the calculated hfcc values for the cis structure and the observed ones, together with the larger stability of the trans structure,

TABLE 3: Isotropic and Anisotropic hfcc's (G) from PWP86/IGLO-III Calculations for the Product Structures for Al + H_2O and Al + NH_3 Optimized at the QCISD/6-31G(d,p) Level

			Al + H_2O					
	nucleus	A_{iso}	T_{xx}[a]	T_{yy}[a]	T_{zz}[a]	A_x[b]	A_y[b]	A_z[b]
HAlOH-trans, this work	Al	313.5	−14.7	−15.9	30.6	298.7	297.6	344.1
HAlOH-cis, this work		374.2	−15.1	−16.5	31.7	359.1	357.7	405.9
HAlOH-trans, Knight et al.[5]		310.8	−17.1	−18.2	35.3	293.7	292.6	346.1
HAlOH-cis, Knight et al.[5]		378.9	−17.1	−17.8	35.0	361.8	361.1	413.9
observed, Knight et al.[5]		327.2	−10.3	−16.8	27.1	316.9	310.4	354.3
HAlOH-trans, this work	H1	−1.4	−1.2	−3.2	4.3	−4.5	−2.5	3.0
HAlOH-cis, this work		11.4	−0.3	−1.0	1.4	10.3	12.8	11.0
HAlOH-trans Knight et al.[5]		−0.7	−2.9	−1.1	3.9	−3.6	−1.8	3.2
HAlOH-cis Knight et al.[5]		10.0	−0.7	1.4	−0.7	9.3	11.4	9.3
observed, Knight et al.[5]		<1.8	–	–	–	–	–	–
HAlOH-trans, this work	H2	103.7	−1.1	1.5	−0.4	102.6	105.2	103.3
HAlOH-cis, this work		108.3	−1.1	1.5	−0.4	107.2	109.8	107.9
HAlOH-trans, Knight et al.[5]		67.1	−1.4	2.1	−0.7	65.7	69.2	66.4
HAlOH-cis, Knight et al.[5]		67.4	−1.4	2.1	−0.7	66.0	69.5	66.7
observed, Knight et al.[5]		102.8	−0.7	0.7	0.0	102.1	103.5	102.8
			Al + NH_3					
	nucleus	A_{iso}	T_{xx}	T_{yy}	T_{zz}	A_x	A_y	A_z
$HAlNH_2$, this work	Al	332.8	−17.7	−16.3	34.0	315.1	316.5	366.8
observed, Howard et al.[41]		329.2						
$HAlNH_2$, this work	N	10.4	−1.0	−0.3	−1.4	9.4	10.1	11.8
observed, Howard et al.[41]		9.6						
$HAlNH_2$, this work	H1	12.8	−1.2	−0.2	1.4	11.6	12.5	14.2
observed, Howard et al.[41]		9.6						
$HAlNH_2$, this work	H2	86.0	−1.3	−0.3	1.6	84.7	85.7	87.7
observed, Howard et al.[41]		81.6						
$HAlNH_2$, this work	H3	−0.4	−1.6	−0.9	2.5	−2.1	−1.3	2.0
no observed value reported								

[a] T_{xx}, T_{yy}, T_{zz} refer to the anisotropic part of the diagonalized hyperfine tensor. [b] A_x, A_y, A_z refer to the diagonal element of the diagonalized hyperfine tensor.

supports the earlier suggestions[3−5] that the experimentally observed product species is the trans conformer. The calculated hfcc values for the addition complex are far from the experimental values, and it is hence probably not detected in the ESR experiments. Best overall agreement between calculated and experimental isotropic hfcc values is obtained for the trans structure at the PWP86/IGLO-III level. The assignments of the proton and Al splittings are the following at this level: Al, exptl value 327.2 G, computed 313.5 G; H1, exptl value <2 G, computed −1.4 G; H2, exptl values 102.8 G, computed 103.7 G (cf. Figure 1 and Table 2), giving a maximum deviation between experimental and calculated values of at most 5%.

Isotropic and anisotropic hyperfine coupling constants calculated at the PWP86/IGLO-III//QCISD/6-31G(d,p) level for the aluminum and hydrogen atoms are presented in Table 3. The calculated dipole−dipole couplings for the aluminum atom agree reasonably well with the experimental ones for both the cis and the trans structure, with the values corresponding to the trans structure in slightly better agreement with the experimental ones. Good agreement between calculated and observed values are obtained for H2, whose hyperfine tensor exposes only small anisotropic contributions in the observed as well as calculated values. Its dipole−dipole couplings are identical in the trans and cis structures, and the isotropic contribution is also very similar.

B. Al + NH_3. Employing the same methods as in the aluminum + water study, Sakai calculated the insertion barrier in the Al + NH_3 reaction to be 26−28 kcal/mol.[1] In an experimental study of the reaction of ground-state Al atoms with NH_3, Howard et al. detected four different species.[42] Two were assigned to the $Al(NH_3)_2$ and $Al(NH_3)_4$ complexes, one to the $HAlNH_2$ insertion product, and one to the HAlOH product. The last product was believed to be formed due to the presence of H_2O. We here focus on the Al + NH_3 insertion reaction and on the geometrical and electronic structures of the insertion product.

1. Geometry Optimizations. One addition complex (AC), one insertion product, and one transition state were found at all levels employed for the geometry optimizations, MP2/6-31G(d,p), QCISD/6-31G(d,p), and B3LYP/6-31G(d,p) (Figure 2).

The geometries are nearly independent of the choice of method. The largest difference is found in the Al−N distance in the transition state, which is 1.99 Å at the MP2 level and 2.03 Å at the B3LYP level. The addition complex is close to C_{3v} symmetry, the differences in N−H bond lengths and H−N−Al angles being at most 0.001 Å and 5.6°. In the transition state connecting the addition complex with the insertion product, the interaction between the aluminum atom and NH_3 shortens the Al−N distance and elongates one of the N−H bonds compared to the addition complex. The product, in which the aluminum atom is inserted between the nitrogen atom and one of the hydrogens, is planar at all levels of approximation presently employed.

The products and transition states were verified to be true energy minima and saddle points of first order, respectively, in frequency calculations performed at the MP2/6-31G(d,p) and B3LYP/6-31G(d,p) levels.

As in the case of the Al + H_2O system, IRC[39,40] calculations were performed at the MP2/6-31G(d,p) level and the points connected via TS1 were confirmed to be the Al−NH_3 addition complex and the $HAlNH_2$ insertion product.

2. Potential Energy Surface. The relative energies of the three stationary points are listed in Table 4. As in the case of the Al−H_2O addition complex, the stability of the Al−NH_3 complex is rather similar at all computational levels: 9.5 kcal/mol below the reactants at the B3LYP/6-311+G(2df,p) level

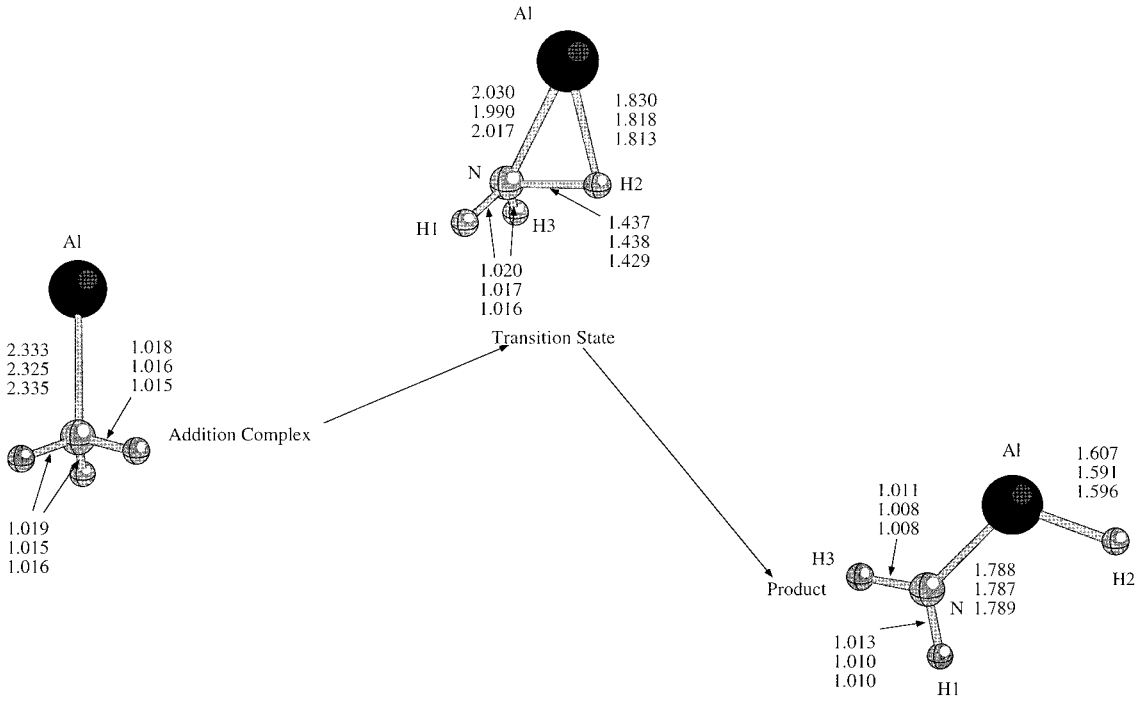

Figure 2. Stationary points on the Al + NH_3 potential energy surface.

TABLE 4: Energies for the Addition Complex, Transition State, and Product on the Al + NH_3 PES at the MP2/6-311+G(2df,p)//MP2/6-31G(d,p),[a] B3LYP/6-311+G(2df,p)//B3LYP/6-31G(d,p),[b] QCISD/6-31G(d,p),[c] and CCSD(T)/6-31G(d,p)//QCISD/6-31G(d,p)[d] Levels of Theory. Energies Are Given in kcal/mol Relative to the Reactants Al and NH_3

	addition complex	transition state	product
MP2	−11.3	17.9	−36.8
MP2, corr.[e]	−8.8	18.3	−36.5
PMP2	−11.7	15.5	−36.2
PMP2, corr.[e]	−9.1	16.0	−35.9
B3LYP	−9.5	13.6	−32.4
B3LYP, corr.[e]	−7.8	9.3	−33.7
QCISD	−12.3	21.2	−26.6
CCSD(T)	−13.0	20.2	−27.5

[a] Absolute energies of the reactants (au): MP2, −298.505608; PMP2, −298.507077. [b] Absolute energies of the reactants (au): B3LYP, −298.970792. [c] Absolute energies of the reactants (au): QCISD, −298.299553. [d] Absolute energies of the reactants (au): CCSD(T), −298.303474. [e] The values are corrected for BSSE employing the 6-311+G(2df,p) basis and ZPE employing the 6-31G(d,p) basis; see text.

and 13.5 kcal/mol at the CCSD(T)/6-31G(d,p) level, respectively. The transition state, in which the migrating hydrogen is halfway between the aluminum and nitrogen atoms, is 13.6 kcal/mol above the reactants at the B3LYP level and 2−8 kcal/mol higher at the (P)MP2, QCISD, and CCSD(T) levels (Table 4). The insertion barrier hence varies between 23 kcal/mol (B3LYP) and 33.5 kcal/mol (QCISD). The insertion product is found to be most stable at the PMP2 level and least at the QCISD level, the numbers being 36 and 27 kcal/mol below the reactants in energy, respectively.

Corrections for BSSE and ZPE were included in the analysis of the reaction profile employing the same methods as for the Al + H_2O system. The estimated BSSE corrections destabilized all stationary points on the PES by 1.7−2.5 kcal/mol at the (P)-MP2 levels and by 0.7−1.0 kcal/mol at the B3LYP level. The ZPE correction stabilized the transition state and product structures by 2 kcal/mol and destabilized the addition complex by 1 kcal/mol at the MP2 level. The ZPE correction calculated at the B3LYP level lowers the energy of the transition state structure 5 kcal/mol. For the product and addition complex the correction is about the same as at the MP2 level.

When both BSSE and ZPE corrections are included, all minima and the transition state are destabilized by 0.3−2.6 kcal/mol at the (P)MP2 levels. The insertion barrier is reduced by 2.1 kcal/mol both at the MP2 and PMP2 levels, to 27.1 and 25.1 kcal/mol, respectively.

Including the BSSE correction and the ZPE corrections at the B3LYP level, the transition state and insertion product are stabilized by 4.3 and 1.3 kcal/mol, respectively; the addition complex on the other hand is destabilized by 1.7 kcal/mol, and the insertion barrier is reduced to 17.1 kcal/mol (cf. Table 4).

Only small differences in energy are seen comparing the MP2 and PMP2 levels for all stationary points, also for the transition state. The value of $\langle S^2 \rangle$ is as in the previous section at most 0.78, except for the transition state, for which a somewhat larger value of 0.84 is found at the MP2 level. The same trends regarding the value of $\langle S^2 \rangle$ are seen as in the case of the Al + H_2O system.

3. Hyperfine Coupling Constants. Reasonable agreement between experimental and calculated isotropic hfcc are seen for all methods using the corresponding product geometry. The only exception is the H2 result at the QCISD level, which is too low compared to the experimental data (cf. Table 5). Values in excellent agreement with experiment are found for H1 at the QCISD and MP2 levels; the corresponding values at the B3LYP and PWP86 levels, on the other hand, are somewhat too large. In the work by Howard et al. an observed quartet pattern of superhyperfine interactions was suggested to arise through coupling to one N(I=1) and one H nucleus with equal coupling constants. This assignment is in the present work supported by the calculated hfcc's of N and H1, which are found to be of similar size at all levels. The assignment of the experimentally observed proton and Al isotropic hfcc are at the B3LYP level of theory as follows: Al, exptl value 329.2 G, computed 324.6 G; N, exptl value 9.6 G, computed 10.3 G; H1, exptl value 9.6

TABLE 5: Isotropic hfcc's (G) for the Addition Complex and Product of the Al + NH_3 System. The Coupling Constants Are Calculated at the MP2/6-311+G(2df,p)//MP2/6-31G(d,p), B3LYP/6-311+G(2df,p)//B3LYP/6-31G(d,p), PWP86/IGLO-III//QCISD/6-31G(d,p), and QCISD/6-311+G(2df,p)//QCISD/6-31G(d,p)[a] Levels of Theory. Included are Experimental Values Taken from the Work by Howard et al.[41]

	structure	Al	N	H1	H2	H3
MP2	addition complex	−31.0	−3.6	1.9	5.5	0.7
	product	325.0	8.5	9.4	64.5	0.5
B3LYP	addition complex	−15.2	−0.4	1.9	6.5	0.7
	product	324.6	10.3	11.8	83.6	−0.6
PWP86	product	332.8	10.4	12.8	86.0	−0.4
QCISD	addition complex	−13.9	−1.32	5.42	1.1	1.1
	product	319.2	8.6	9.7	68.9	−0.6
exptl		329.2	9.6	9.6	81.6	

[a] The calculated hfcc for the addition complex at the QCISD level is performed employing the 6-31G(d,p) basis.

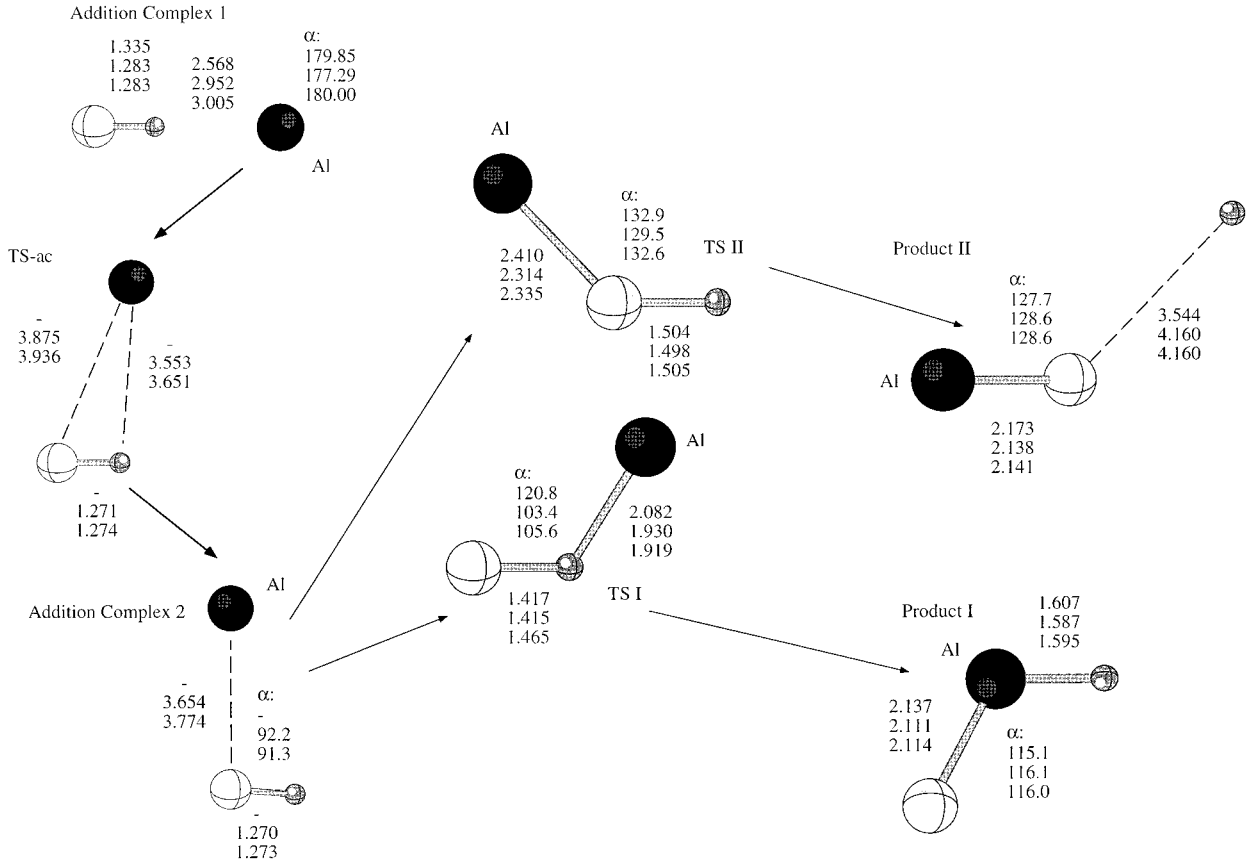

Figure 3. Stationary points on the Al + HCl potential energy surface.

G, computed 11.8 G; and H2, exptl value 81.6 G, computed 83.6 G (cf. Figure 1 and Table 5).

The anisotropic hyperfine coupling constants are presented in Table 3. For the insertion product the calculated hyperfine tensors for N, H1, and H2 show only minor anisotropic contributions. This agrees well with the experimental observation that all the tensors are isotropic. The magnitudes of the calculated anisotropic coupling constants are at most 1.6 G. A noticeable anisotropy is seen in the calculated values for the aluminum hyperfine tensor which is not observed in the experiments. The Al dipole−dipole contribution might, however, be averaged to zero at the experimental temperature of 77 K. The isotropic value for the aluminum atom is, on the other hand, in excellent agreement with the experimental value, indicating a good description of the electronic structure in the vicinity of the aluminum nucleus.

C. Al + HCl and Al + Cl_2. In a recent matrix isolation ESR study, isotropic and anisotropic hfcc values for the products of the Al + Cl_2 and Al + HCl reactions were determined.[6] In the same work, the MNDO method was furthermore employed in a theoretical study of the Al + HCl reaction. On the basis of the calculations, it was suggested that this reaction occurs spontaneously and that the outcome of the reaction depends upon which end of the HCl molecule the Al atom attacks. If the Al atom approaches the hydrogen end, an HAlCl insertion product is formed, whereas if the attack is on the chlorine side, a displacement reaction occurs in which the hydrogen atom is removed, leaving an AlCl molecule.

1. Geometry Optimizations. Two addition complexes, one linear (AC1) and one bent (AC2), were found at the MP2/6-31G(d,p) and QCISD/6-31G(d,p) levels. Only AC1 was found at the B3LYP/6-31G(d,p) level of approximation. For both complexes the aluminum atom binds loosely to HCl, interacting with the hydrogen side of HCl in AC1 and mainly with the chlorine atom in AC2, respectively (cf. Figure 3). Also a transition state connecting the two addition complexes (TS-ac) was found at the ab initio levels (cf. Figure 3). However neither

TABLE 6: Energies for Addition Complex, Transition States, and Product Optimized for the Al + HCl Reaction at MP2/6-311+G(2df,p)//MP2/6-31G(d,p),[a] B3LYP/6-311+G(2df,p)//B3LYP/6-31G(d,p),[b] QCISD/6-31G(d,p),[c] and CCSD(T)/6-31G(d,p)//QCISD/6-31G(d,p)[d] Levels of Theory. Energies Are Given in kcal/mol Relative to the Reactants Al and HCl

	AC1	TS-ac	AC2	TS I	product I	TS II	product II[f]
MP2	−3.4	−1.92	−2.0	−1.2	−56.5	7.5	−21.6
MP2, corr.[e]	−2.9	−1.42	−1.7	−1.5	−54.5	6.0	
PMP2	−3.5	−1.95	−2.1	−2.5	−56.0	4.9	−20.7
PMP2, corr.[e]	−3.0	−1.41	−1.8	−2.8	−53.9	3.4	
B3LYP	−4.5			−3.2	−51.5	2.4	−12.4
B3LYP, corr.[e]	−4.8			−4.5	−50.9	−0.2	
QCISD	−2.3	−1.1	−1.1	6.7	−45.8	16.3	−12.6
CCSD(T)	−2.4	−1.2	−1.2	5.1	−46.5	14.2	−13.6

[a] Absolute energies of the reactants (au): MP2, −702.397465; PMP2, −702.398934. [b] Absolute energies of the reactants (au): B3LYP, −703.223508. [c] Absolute energies of the reactants (au): QCISD, −702.122858. [d] Absolute energies of the reactants (au): CCSD(T), −702.125932. [e] The values are corrected for BSSE employing the 6-311+G(2df,p) basis and ZPE employing the 6-31G(d,p) basis; see text. [f] The energy of product II is the energy of AlCl plus the energy of a hydrogen atom.

this transition state nor AC2 was in our calculations possible to localize at the B3LYP level.

One product structure in which the aluminum atom is inserted into the H−Cl bond was located (cf. Figure 3). The geometry of the product structure is similar at all levels, with the longest Al−Cl and Al−H bonds being obtained at the B3LYP level and the shortest ones at the MP2 level. The difference between the two levels is 0.03 Å for the Al−Cl bond and 0.02 Å for the Al−H bond.

Two transition states were located at all levels employed: one in which Al binds to hydrogen (TS I) and a second one in which Al binds to chlorine (TS II). Somewhat larger method dependencies than the ones found for the products are seen for the two transition states. For TS I, B3LYP predicts an earlier transition state than MP2/QCISD, with a larger H−Cl−Al angle and a longer Al−Cl bond. A similar, but not as pronounced, trend is also observed for TS II (cf. Figure 3). As mentioned earlier, a third transition state (TS-ac) connecting the two addition complexes was also found at the MP2 and QCISD levels. All points were verified to be true energy minima or transition states through frequency calculations at the B3LYP and MP2 levels.

Also IRC calculations were performed at the MP2 level starting from the three transition states. The points connected via TS-ac were confirmed to be AC1 and AC2. The points connected via TS I were confirmed to be the AC2 and the insertion product (product I), and finally the points connected via TS II were AC2 and the aluminum chloride without the hydrogen (product II). Passing over TS II is thus a reaction in which the attack of the aluminum atom on HCl results in the removal of the hydrogen. Note that the starting point in both reactions is AC2.

2. Potential Energy Surface. The relative energies of the six stationary points optimized at the different levels of approximation are displayed in Table 6. The addition complex AC1 is most stable at the B3LYP/6-311+G(2df,p)//6-31G(d,p) level and least at the QCISD/6-31G(d,p) level, 4.5 and 2.3 kcal/mol below the reactants in energy, respectively.

The transition state connecting the two addition complexes (TS-ac) is 1.9 kcal/mol below the reactants at the (P)MP2 levels and 1.1 kcal/mol below at the QCISD level, respectively. This results in a barrier of only a few tenths of a kcal/mol when going from AC2 to AC1. At the QCISD level this barrier is as small as 0.01 kcal/mol. Since DFT methods often predict lower energy barriers compared to ab initio,[43−45] it is not surprising that the small energy barrier separating AC2 from AC1 vanishes at the B3LYP level. Because of this very small energy difference between AC2 and TS-ac, AC2 was not considered as a stationary point at the PES but as a plateau, and the energy barriers for both reactions (insertion and hydrogen removal) are calculated using AC1 as the common starting point at all levels of approximation.

The first transition state (TS I), in which the aluminum atom binds to the hydrogen, is 3.2 kcal/mol below the reactants at the B3LYP level and 6.7 kcal/mol above the reactants at the QCISD level, respectively. This results in an Al insertion barrier at the QCISD level of 9.0 kcal/mol if AC1 is taken as the starting point. The barrier is reduced to 7.5 and 2.2 kcal/mol at the CCSD(T) and MP2 levels, respectively, and drops further to 1.0 kcal/mol at the PMP2 level. At the B3LYP level the barrier to reach the insertion product is 1.3 kcal/mol (Table 6). The insertion product is found to be 56 kcal/mol below the reactants in energy at the (P)MP2 levels, 51 kcal/mol at the B3LYP level, and 46 kcal/mol at the QCISD level, respectively. The barrier for the removal of the hydrogen atom, passing over transition state II, is larger than the insertion barrier, being 7−11 kcal/mol at the (P)MP2 and B3LYP levels and 18.6 kcal/mol at the QCISD level.

Finally, corrections for BSSE and ZPE were included (using the same methods as in the previous sections) in the analysis of the reaction profile. Including the BSSE corrections, the stationary points were destabilized by 0.3−0.5 kcal/mol (the addition complex), 0.6−2.1 kcal/mol (the insertion product), and 0.6−1.9 kcal/mol (transition states), at the different levels of approximation.

The ZPE correction stabilized the transition states by 2−3 kcal/mol, while the addition complex and insertion product were almost unaffected. The ZPE correction calculated at the B3LYP level influences the stationary points in a similar way as at the (P)MP2 levels; the transition states were stabilized by 1.5−3 kcal/mol, whereas the addition complex and insertion product were stabilized by less than 0.5 kcal/mol.

Including both corrections in the energy profile causes only minor changes in the stability of the addition complexes and TS I at the (P)MP2 levels: The addition complexes are destabilized by 0.3−0.5 kcal/mol, and TS I is stabilized by 0.3 kcal/mol. The second transition state and the insertion product (product I) are influenced somewhat more by the corrections at this level: TS II is stabilized by 1.5 kcal/mol, and the insertion product (product I) is destabilized by around 2 kcal/mol. Including the corrections, the values for the insertion barrier are 1.4 and 0.2 kcal/mol at the MP2 and PMP2 levels, respectively. The corresponding numbers for the barrier leading to the removal of the hydrogen are 8.9 and 6.4 kcal/mol.

At the B3LYP level only small changes are observed for the addition complex as well as the insertion product when the BSSE and ZPE corrections are included. TS I and TS II are stabilized somewhat more: by 1.3 and 2.6 kcal/mol, respectively

TABLE 7: Isotropic hfcc's (G) for the Addition Complex and Product of the Al + HCl System. The Coupling Constants Are Calculated at the MP2/6-311+G(2df,p)//MP2/6-31G(d,p), B3LYP/6-311+G(2df,p)//B3LYP/6-31G(d,p), PWP86/IGLO-III//QCISD/6-31G(d,p), and QCISD/6-311+G(2df,p)//QCISD/6-31G(d,p)[a] Levels of Theory. Included Are the Original Experimental Assignments[6]

	structure	H	Al	Cl
MP2	addition complex I	−2.5	−15.7	−7.4
	addition complex II	0.4	−20.0	−0.9
	insertion product	82.9	368.6	10.3
B3LYP	addition complex I	1.6	−22.5	17.9
	addition complex II			
	insertion product	106.9	370.2	9.6
PWP86	insertion product	106.6	370.5	10.8
QCISD	addition complex I	−5.3	−5.0	5.1
	addition complex II	0.3	−13.8	−0.3
	insertion product	88.6	361.2	10.5
exptl		100.8	400.1	(−7.4)

[a] The hfcc's for the addition complex are calculated employing the 6-31G(d,p) basis.

(cf. Table 6). The corrected barriers at the B3LYP level are 0.3 kcal/mol (insertion barrier) and 4.6 kcal/mol (hydrogen removal).

The same trends regarding the value of $\langle S^2 \rangle$ are seen as in the case of the Al + H_2O and Al + NH_3 systems.

3. Hyperfine Coupling Constants. The isotropic hfcc values were calculated for the insertion product employing the same methods as for the AlH_2O and $AlNH_3$ systems (cf. Table 7). Somewhat too small calculated couplings are obtained for the aluminum atom, compared to the experimental value. Also the value of the hydrogen coupling at the MP2 and QCISD levels is calculated too low compared to experiments, although the agreement between the experimental and calculated values is reasonable at both levels. The best overall agreement is obtained employing the B3LYP/6-311+G(2df,p)//B3LYP/6-31G(d,p) level (cf. Figure 1c and Table 7). The anisotropic hyperfine coupling constants, calculated as in previous sections, are presented in Table 8. The experimental values of T_{xx}, T_{yy}, and T_{zz} shown in Table 8 are derived from the observed values of A_x, A_y, and A_z reported in the previous experimental work.[6] The calculated anisotropic values for the aluminum atom are in excellent agreement with the experimentally observed values.

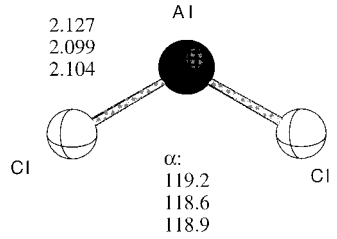

Figure 4. Optimized geometry of the ClAlCl product.

The orientation of the Cl hfc tensor, α, relative to the Al tensor was calculated to be 29°. Both observed and calculated hyperfine tensors for H show only minor anisotropic contributions, the magnitude of the largest calculated anisotropic contribution being at most 1.5 G. The isotropic hfcc of the chlorine atom is calculated too large at all levels compared to the experimental value.

For the chlorine anisotropic components, the observed deviations between the original assignment[6] and present computed data are discussed in greater detail below.

4. Geometrical Structure, Energetic Stability, and hfcc of ClAlCl. A product structure of C_{2v} symmetry, in which the aluminum atom is inserted into the Cl−Cl bond, is obtained at all levels employed for the geometry optimizations of Cl−Al−Cl (cf. Figure 4). The geometry of the product structure is similar at all levels; the Al−Cl bond is 0.03 Å longer and the Cl−Al−Cl angle 0.6° larger at the B3LYP level compared to MP2. The geometry obtained at the QCISD level lies in between those encountered at the other two levels. The Al insertion product is 130, 140, 131, and 131 kcal/mol below the reactants in energy at the B3LYP, MP2, QCISD, and CCSD(T) levels, respectively (cf. Table 9). Only small deviations from the ideal value of $\langle S^2 \rangle$ are seen for the product at the different levels. A maximum value of 0.767 is encountered at the MP2 level.

The calculated isotropic components of the Al hyperfine tensor are in good agreement but somewhat too low compared to the experimental value. At the QCISD level A_{iso}(Al) is, however, far too small compared to the previously estimated experimental value (Table 10). The calculated anisotropic Al components show reasonable, although not perfect, agreement with the observed experimental values (cf. Table 8). The

TABLE 8: Isotropic and Anisotropic hfcc's (G) from PWP86/IGLO-III Calculations for the Product Structures for Al + HCl and Al + Cl_2 Reactions Optimized at the QCISD/6-31G(d,p) Level

Al + HCl

	nucleus	A_{iso}	T_{xx}[b]	T_{yy}[b]	T_{zz}[b]	A_x[c]	A_y[c]	A_z[c]
HAlCl, this work	Al	370.5	30.8	−15.2	−15.6	401.3	355.3	355.0
observed[6]		400	30	−15	−15	430	385	385
HAlCl, this work	H	106.6	1.5	−0.3	−1.1	108.1	106.2	105.4
observed[6]		100				100	100	100
HAlCl, this work	Cl	10.8	11.7	−5.5	−6.2	22.5	5.3	4.6
observed[6a]		−7.3	7.3	−3.7	−3.7	0	−11	−11
observed, this work[d]		11	9	−5	−5	20	6	6

Al + Cl_2

	nucleus	A_{iso}	T_{xx}	T_{yy}	T_{zz}	A_x	A_y	A_z
ClAlCl, this work	Al	543.5	22.8	−10.4	−12.3	578.6	545.4	543.5
observed[6]	Al	573.3	26.7	−13.8	−13.8	600	560	560
ClAlCl, this work	Cl	17.7	15.2	−7.2	−8.0	32.5	10.1	9.3
observed[6a,e]	Cl	−11.3	11.3	−5.7	−5.7	0	−17	−17

[a] Original assignment. See also text, section III C.5. [b] T_{xx}, T_{yy}, T_{zz} refer to the anisotropic part of the diagonalized hyperfine tensor. [c] A_x, A_y, A_z refer to the diagonal element of the diagonalized hyperfine tensor. [d] The reassessed Cl hfc tensor. See also text, section III C.5. [e] The Al hyperfine component 6 of $AlCl_2$ was simulated on the basis of the experimentally determined Al hfc tensor and the *theoretically* determined Cl hfc tensor. The so simulated spectrum is in much better agreement with the observed spectrum compared to the original simulations;[6] see also Figure 7 and text, section III C.5.

TABLE 9: Energies for the Al Insertion Product for $AlCl_2$ at the B3LYP, MP2, QCISD, and CCSD(T) Levels of Theory. Energies Are Given in kcal/mole Relative to the Reactants Al and Cl_2

level	reactants (energy in au)	product
MP2/6-311+G(2df,p)//MP2/6-31G(d,p)	−1161.521 292	−140.8
PMP2/6-311+G(2df,p)//MP2/6-31G(d,p)	−1161.522 761	−140.4
B3LYP/6-311+G(2df,p)//B3LYP/6-31G(d,p)	−1162.810 058	−130.3
QCISD/6-31G(d,p)	−1161.099 521	−131.4
CCSD(T)/6-31G(d,p)//QCISD/6-31G(d,p)	−1161.106 977	−131.5

TABLE 10: Isotropic hfcc's (G) for the Insertion Product of the Al + Cl_2 Reaction. The Coupling Constants Are Calculated at the MP2/6-311+G(2df,p)//MP2/6-31G(d,p), B3LYP/6-311+G(2df,p)//B3LYP/6-31G(d,p), PWP86/IGLO-III//QCISD/6-31G(d,p), and QCISD/6-311+G(2df,p)//QCISD/6-31G(d,p) Levels of Theory. Included Are the Original Experimental Assignments[6]

	structure	Al	Cl
MP2	insertion product	536.1	15.9
B3LYP	insertion product	563.1	14.9
PWP86	insertion product	543.5	17.7
QCISD	insertion product	527.9	16.2
exptl[a]		573.5	((−)11.3)

[a] The Al hyperfine component 6 of $AlCl_2$ was simulated on the basis of the experimentally determined Al hfc tensor and the *theoretically* determined Cl hfc tensor. The so simulated spectrum is in much better agreement with the observed spectrum compared to the original simulations;[6] see also Figure 7 and text, section III C.5.

orientation of the Cl hfc tensors, $\pm\alpha$, relative to the Al tensor was calculated to be $\pm 34°$. The chlorine values, on the other hand, all show large deviations from the original experimental data. QCISD performs best but is still off by as much as 30%, assuming A_{iso}(Cl) to be positive. Best overall agreement for the isotropic hyperfine couplings is obtained employing the B3LYP/6-311+G(2df,p)//B3LYP/6-31G(d,p) method.

5. Spectral Simulations of HAlCl and ClAlCl. Prompted by the theoretical results it was decided to re-examine the Cl hfc tensors of HAlCl and $AlCl_2$.

Figure 5a shows the total spectrum observed from the Al/HCl(2%)/Ar system. The Cl hfs's are most clearly observed with least interference from other signals for component 5 of the aluminum hfs of the HAlCl spectrum and component 6 of the $AlCl_2$ spectrum (counting the hf components from the low-field end). These components are shown expanded in Figure 6b and Figure 7a, respectively.

In the earlier analysis[6] it was suggested that the Cl hfs resolved here corresponded to the direction perpendicular to the molecular plane of the respective species, as the relevant principal axes of the *g* tensor and all the hfc tensors involved coincide only in that direction. Since the Cl hfc tensor is expected to be approximately axially symmetric about the Al−Cl internuclear direction, the observed spacing was identified with $A_\perp$. $A_\parallel$ was then determined to yield the best fit with the observed overall pattern.

Figure 5b shows the simulated ESR powder pattern based on the *g* tensor and only the Al hfc tensor observed from HAlCl. It is immediately clear that the component 3 is almost totally free from the anisotropy of the Al hfc tensor. Component 3 of HAlCl actually observed is shown expanded in Figure 6a. The anisotropy of the H hfc tensor is negligibly small. It then follows that the spectral pattern observed here is a pure manifestation of the Cl hfc tensor.

In Figure 6a one may recognize that each component of the hydrogen doublet has an appearance of a quartet of unequal

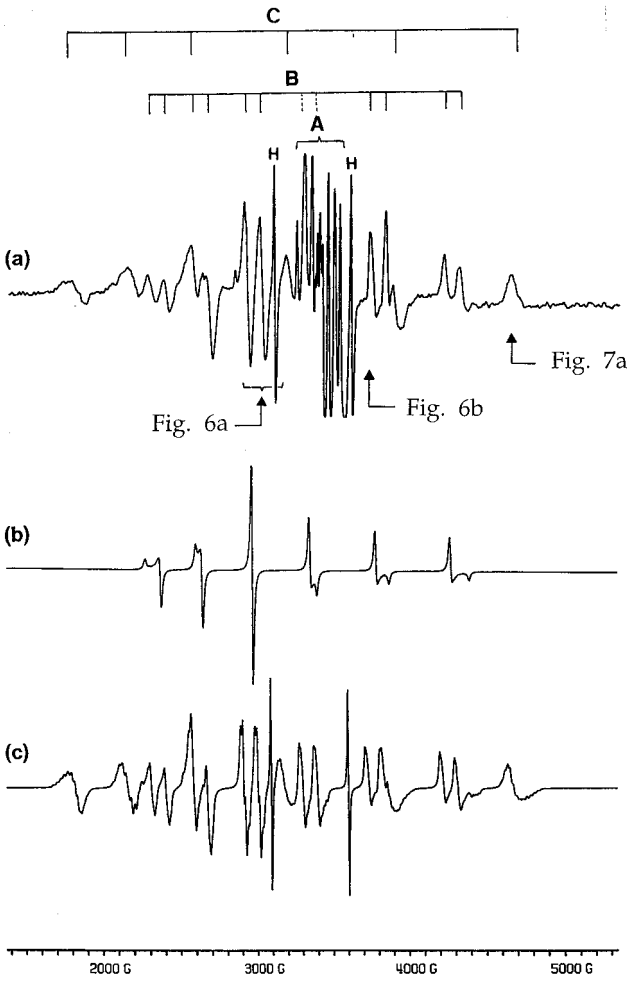

Figure 5. (a) Entire ESR spectrum observed from the Al/HCl(2%)/Ar system. The doublet indicated by letter H is due to H atoms. Signals A are due to isolated Al atoms. The sextet of doublet B and the sextet C are assigned to HAlCl and $AlCl_2$, respectively. (b) ESR powder pattern simulated based on the *g* tensor and only the Al hfc tensor determined from the HAlCl spectrum. (c) Overall spectral pattern simulated based on the *g* tensors, the Al and H coupling tensors determined previously (ref 6), and the presently determined/calculated Cl hfc tensors. The relative molar concentrations of 1/0.5/0.03 were assumed for HAlCl, $AlCl_2$, and H atoms, respectively.

intensity and its outermost components (indicated by arrows) have the shapes characteristic of the parallel components. These peaks are hence assigned to the outermost components of the quartet due to the Cl hfs in the parallel direction. Thus $A_\parallel = 20 \pm 2$ G. The Cl $A_\perp$ may then be determined as that which would give the best fit for the Al hyperfine component 3. We thus determined $A_\perp = 6 \pm 1$ G. Figure 6c shows the computed Al hf component 3 based on the *g* tensor, the Al and H hfc tensors determined earlier, and the Cl hfc tensor reassessed presently. The Cl hfc tensor presently determined is in excellent agreement with that given by the PWP86/IGLO-III method (Table 8).

Figure 6b shows the Al hf component 5. The observed Cl hfs has spacings of 11 G. These spacings are attributed to the combined effect of the anisotropy of the Al and Cl hfc tensors and their relative orientation. Using the complete set of tensors as described above, the orientation of the Cl hfc tensor, α, relative to the Al hfc tensor was determined as that which would give the best fit with the observed (Figure 6d). We thus obtained $\alpha = 30 \pm 5°$. The sensitivity of the pattern upon the relative orientation is illustrated in Figure 8, where the spectra

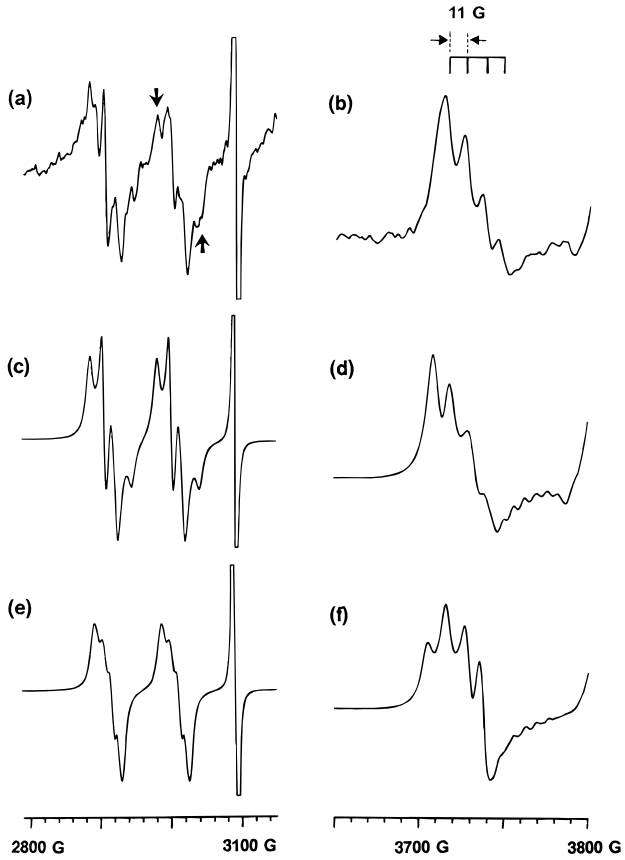

Figure 6. (a) Al hf component 3 of HAlCl (of Figure 5a) shown in an expanded scale. (b) Al hf component 5 of HAlCl shown in an expanded scale. (c) Computed Al hf component 3 based on the *g* tensor, the Al and H hfc tensors determined earlier (ref 6), and the Cl hfc tensor presently reassessed. (d) Simulated Al hf component 5 based on the complete set of tensors used in (c) and $\alpha = 30°$, the orientation of the Cl hfc tensor relative to the Al hfc tensor. (e) Al hf components 3 and 5 simulated using the Cl hfc tensor previously reported (ref 6). (f) Al hf components 3 and 5 simulated using the Cl hfc tensor previously reported (ref 6).

simulated for $\alpha = 0°$, 15°, 30°, and 45° are shown. Figure 6e,f shows, respectively, the Al hf components 3 and 5 simulated using the Cl hfc tensor previously reported.

For $AlCl_2$ a similar analysis revealed that the Al hf component 3 is also free from the anisotropy of the Al hfc tensor. However, the component 3 of $AlCl_2$ was masked by component 2 of HAlCl, and the Cl hfc tensor of $AlCl_2$ could not be determined in the explicit manner available for HAlCl.

Figure 7a shows the Cl hfs revealed in the Al hf component 6 of $AlCl_2$ observed from the Al/HCl(2%)/Ar system. The pattern is characterized by a multiplet of unequal intensity with successive spacings of 17 G. Relying on the excellent agreement noted between the theoretically and experimentally determined Cl hfc tensors of HAlCl, the Al hyperfine component 6 of $AlCl_2$ was simulated on the basis of the experimentally determined Al hfc tensor, the theoretically determined Cl hfc tensor ($A_{||} = 30$ G and $A_{\perp} = 10$ G), and the assumed relative orientations of the tensors given by $\pm\alpha$. The best agreement was obtained for $\alpha = \pm 40°$ (Figure 7b). For comparison, Figure 7c shows the spectrum simulated using the previously reported Cl hfc tensor. As can be seen, Figure 7b is in much better agreement with the observed spectrum.

Figure 5c shows, finally, the overall spectral pattern simulated by means of the *g* tensors, the Al and H coupling tensors determined previously, and the presently determined/calculated

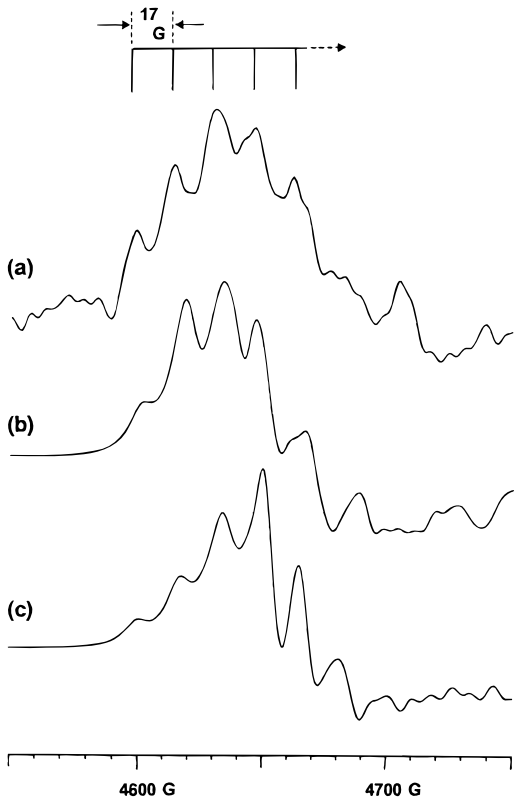

Figure 7. (a) Al hf component 6 of $AlCl_2$ (of Figure 5a) shown in an expanded scale. (b) Al hf component 6 simulated based on the theoretically determined Cl hfc tensor and the orientations of $\pm 40°$ for the two Cl hfc tensors relative to the Al hfc tensor. (c) Al hf component 6 simulated using the previously reported Cl hfc tensor (ref 6).

Cl hfc tensors. The relative molar concentrations of 1/0.5/0.03 were assumed for HAlCl, $AlCl_2$, and H atoms, respectively.

IV. Summary and Conclusion

Stationary points on the surface describing the reaction between Al and H_2O, NH_3, HCl, and Cl_2 have been optimized at the MP2, B3LYP, and QCISD levels using the 6-31G(d,p) basis set. Reaction energies were calculated using B3LYP, MP2 methods, and QCISD and CCSD(T) methods in conjunction with the 6-311+G(2df,p) and 6-31G(d,p) basis sets, respectively. Isotropic hyperfine coupling constants (hfcc's) of Al, N, Cl, and the protons were computed using MP2, QCISD, and B3LYP methods in conjunction with the 6-311+G(2df,p) basis for isotropic hyperfine couplings and at the PWP86/IGLO-III level for isotropic and anisotropic coupling constants. Also, new spectral simulations have been performed for the HAlCl and ClAlCl systems using the presently determined/calculated Cl hfc tensors.

A. Energetic Stability. The most stable addition complex is found for the Al + NH_3 reaction, this complex being 9−14 kcal/mol below the reactants depending on method; the corresponding numbers for the Al + H_2O and Al + HCl reactions are 5−9 kcal/mol and 2−4 kcal/mol, respectively. The addition complexes were found to be most stable at the CCSD(T) and least at the B3LYP level for the Al + H_2O and Al + NH_3 systems, while the opposite situation was found for the AlHCl addition complex (AC1).

For the Al + H_2O reaction, two insertion products, one cis and one trans (35−45 kcal/mol below the reactants, depending on method), were found, with the trans product about 1 kcal/mol more stable compared to the cis, irrespectively of the

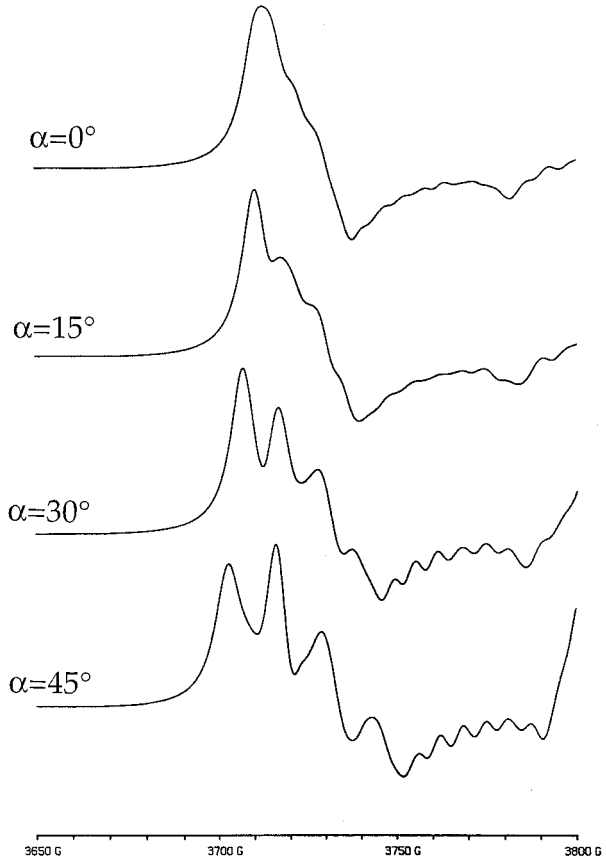

Figure 8. Al hf component 5 of HAlCl simulated based on the *g* tensor, the Al and H hfc tensors determined earlier (ref 6), and the Cl hfc tensor presently reassessed with the indicated orientation of the Cl hfc tensor relative to the Al hfc tensor.

method used. In the Al + NH_3 reaction, a planar insertion product was localized 25−35 kcal/mol below the reactants, and in the Al + HCl reaction the insertion product was found to be stabilized 45−55 kcal/mol compared to the reactants. A second reaction path was localized for the latter reaction, leading through a removal of the hydrogen to the formation of AlCl, 10−20 kcal/mol below the reactants in energy with an energy barrier of 5−20 kcal/mol, depending on method. Thus the calculated energetics for the Al + HCl system favors the formation of the insertion product. The most stable insertion product encountered is the ClAlCl product, this product being 130−140 kcal/mol below the reactants in energy. All products in all reactions are predicted to be most stable at the MP2 level and least at the QCISD level with the one exception of the ClAlCl system, for which the MP2 level predicts the most stable insertion product and the B3LYP the least.

The lowest energy barrier for the insertion reactions is reported for the Al + HCl system, in which the barrier nearly vanishes when ZPE and BSSE corrections are included; however both the CCSD(T) and QCISD methods support the existence of an energy barrier of 7−10 kcal/mol for this insertion reaction. A somewhat larger insertion barrier is found for the Al−H_2O reaction: the barrier varies between 7.8 and 12.7 kcal/mol (corrected) depending on method. The largest insertion energy barrier in the present study is reported for the Al−NH_3 reaction with a barrier height ranging from 17.1 to 27.1 kcal/mol (corrected) depending on method. In general, including the BSSE and ZPE corrections the energy barriers are reduced by a few kilocalories per mole. Overall, the B3LYP method predicts the lowest energy barriers and the QCISD and CCSD-(T) methods the highest. The one exception is the small energy barrier for the Al + HCl reaction, in which the PMP2 method gives an energy barrier that is a few tenths of a kcal/mol smaller than the B3LYP barrier. The energetics predicted for the different reactions, employing the CCSD(T) and QCISD methods, are without exception very similar.

B. hfcc and Spectral Simulations. For the Al + H_2O reaction, the best overall agreement between calculated and experimental isotropic hfcc values is obtained for the trans structure at the PWP86/IGLO-III//QCISD/6-31G(d,p) level, the maximum deviation between experimental and calculated values being at most 5%. Reasonable agreement between the calculated and observed dipole−dipole couplings for the aluminum atom is observed for both the cis and trans structure, with the values corresponding to the trans structure in slightly better agreement with the experimental ones. The two hydrogen hyperfine tensors expose only small anisotropic contributions both in the calculated and experimentally observed values.

Both hfcc and energetic considerations support, as in previous works by Knight et al.[5] and Joly et al.,[4] the HAlOH-trans structure to be the final product in the Al + H_2O reaction.

Reasonable agreement between calculated and observed isotropic hfcc's was in the present study reported for the Al + NH_3 insertion product. Best agreement between calculated and experimental values was observed for the B3LYP/6-311+G-(2df,p)//B3LYP/6-31G(d,p) level, with an average deviation between experimental and calculated values of 9.4%.

Reasonable agreement was also observed for the calculated and experimental aluminum and proton isotropic hfcc values for the AlHCl system. Again, best agreement was found at the B3LYP/6-311+G(2df,p)//B3LYP/6-31G(d,p) level, with an average deviation of 7%. Both observed and calculated hyperfine tensors for the proton show only minor anisotropic contributions, the magnitude of the largest calculated contribution being at most 1.5 G. The present theoretical work prompted a reassessment of the Cl hfc tensor. An excellent agreement now exists between the computed tensor and that reassessed from the spectrum. Very good agreement is also observed between the relative orientation of the Al and Cl tensors, α, obtained in the spectral simulations ($\alpha = 30 \pm 5°$) and in the calculations ($\alpha = 29°$).

Also for ClAlCl the calculated isotropic component of the Al hyperfine tensor at the B3LYP/6-311+G(2df,p)//B3LYP/6-31G(d,p) level is in very good agreement with the experimental values. On the other hand, the theoretical findings predict an Cl hf tensor at variance with the previously reported experimental values. Again, performing new spectral simulations based on the experimentally determined Al hfc tensor, the theoretically determined Cl hfc tensor, and a relative orientation of the tensors of ±40°, a much better agreement between the simulated and observed spectra was again noted compared to the previously performed spectral simulations. Again good agreement was seen between calculated ($\alpha = \pm 34°$) and in the spectral simulations obtained ($\alpha = \pm 40°$) relative orientation of the Al and Cl tensors.

Small and highly anisotropic hfc tensors and their relative orientations determined by accurate theoretical methods can greatly facilitate and/or substantiate the analyses of ESR powder patterns.

Acknowledgment. The Swedish Natural Sciences Research Council (NFR) is gratefully acknowledged for financial support. Grants of computer time on the IBM SP at the Center for Parallel Computers (PDC) in Stockholm and the Cray C90 of the

Swedish Supercomputer Center (NSC) in Linköping are gratefully acknowledged.

References and Notes

(1) Sakai, S. *J. Phys. Chem.* **1992**, *96*, 8369.
(2) Sakai, S. *J. Phys. Chem.* **1993**, *97*, 8917.
(3) Cramer, C. J. *J. Mol. Struct. (THEOCHEM)* **1991**, *235*, 243.
(4) Joly, H. A.; Howard, J. A.; Tomietto, M.; Tse, J. S. *J. Chem. Soc., Faraday Trans.* **1994**, *90*, 3145.
(5) Knight, L. B., Jr.; Gregory, B.; Cleveland, J.; Arrington, C. A. *Chem. Phys. Lett.* **1993**, *204*, 168.
(6) Köppe, R.; Kasai, P. H. *J. Am. Chem. Soc.* **1996**, *118*, 135.
(7) Frisch, M. J.; Trucks, G. W.; Schlegel, H. B.; Gill, P. M. W.; Johnson, B. G.; Wong, M. W.; Foresman, J. B.; Robb, M. A.; Head-Gordon, M.; Replogle, E. S.; Gomperts, R.; Andres, J. L.; Raghavachari, K.; Binkley, J. S.; Gonzalez, C.; Martin, R. L.; Fox, D. J.; Defrees, D. J.; Baker, J.; Stewart, J. P.; Pople, J. A. *Gaussian 92/DFT, Revision G.3*; Gaussian, Inc.: Pittsburgh, PA, 1993.
(8) Frisch, M. J.; Trucks, G. W.; Schlegel, H. B.; Gill, P. M. W.; Johnson, B. G.; Robb, M. A.; Cheeseman, J. R.; Keith, T.; Petersson, G. A.; Montgomery, J. A.; Raghavachari, K.; Al-Laham, M. A.; Zakrzewski, V. G.; Ortiz, J. V.; Foresman, J. B.; Cioslowski, J.; Stefanov, B. B.; Nanayakkara, A.; Challacombe, M.; Peng, C. Y.; Ayala, P. Y.; Chen, W.; Wong, M. W.; Andres, J. L.; Replogle, E. S.; Gomperts, R.; Martin, R. L.; Fox, D. J.; Binkley, J. S.; Defrees, D. J.; Baker, J.; Stewart, J. P.; Head-Gordon, M.; Gonzalez, C.; Pople, J. A. *Gaussian 94, Revision B.2*; Gaussian, Inc.: Pittsburgh, PA, 1995.
(9) Møller, C.; Plesset, M. S. *Phys. Rev.* **1934**, *46*, 618.
(10) Pople, J. A.; Head-Gordon, M.; Raghavachari, K. *J. Chem. Phys.* **1987**, *87*, 5968.
(11) Slater, J. C. *Quantum Theory of Molecular and Solids Vol 4: The Self-Consistent Field for Molecular and Solids*; McGraw-Hill: New York, 1974.
(12) Fock, V. *Z. Phys.* **1930**, *61*, 126.
(13) Becke, A. D. *Phys. Rev. A* **1988**, *38*, 3098.
(14) Wilk, L.; Vosko, S. H.; Nusair, M. *Can. J. Phys.* **1980**, *58*, 1200.
(15) Lee, C.; Yang, W.; Parr, R. G. *Phys. Rev. B* **1988**, *37*, 785.
(16) Hariharan, P. C.; Pople, J. A. *Theor. Chim. Acta* **1973**, *28*, 213.
(17) Francl, M. M.; Petro, W. J.; Hehre, W. J.; Binkley, J. S.; Gordon, M. S.; Defrees, D. J.; Pople, J. A. *J. Chem. Phys.* **1982**, *77*, 3654.
(18) Krishnan, R.; Binkley, J. S.; Seeger, R.; Pople, J. A. *J. Chem. Phys.* **1980**, *72*, 650.
(19) McLean, A. D.; Chandler, G. S. *J. Chem. Phys.* **1980**, *72*, 5639.
(20) Clark, T.; Chandrasekhar, J.; Spitznagel, G. W.; Schleyer, P. von R. *J. Comput. Chem.* **1983**, *4*, 294.
(21) Gill, P. M. W.; Johnson, B. G.; Pople, J. A.; Frisch, M. J. *Chem. Phys. Lett.* **1992**, *197*, 499.
(22) Frisch, M. J.; Pople, J. A.; Binkley, J. S.; Schleyer, P. von R. *J. Chem. Phys.* **1984**, *80*, 3265.
(23) Pople, J. A.; Head-Gordon, M.; Raghavachari, K. *J. Chem. Phys.* **1987**, *87*, 5968.
(24) Fermi, E. *Z. Phys.* **1930**, *60*, 320.
(25) Fermi, E.; Segre, E. *Z. Phys.* **1933**, *82*, 729.
(26) Perdew, J. P.; Wang, Y. *Phys. Rev.* **1986**, *B33*, 8800.
(27) Perdew, J. P. *Phys. Rev. B* **1986**, *33*, 8822.
(28) Perdew, J. P. *Phys. Rev.* **1986**, *34*, 7406.
(29) Kutzelnigg, W.; Fleischer, U.; Schindler, M. *NMR−Basic Principles and Progress*; Springer-Verlag: Heidelberg, 1990; Vol. 23.
(30) St-Amant, A.; Salahub, D. R. *Chem. Phys. Lett.* **1990**, *169*, 387.
(31) St-Amant, A. Ph.D. Thesis, Université de Montréal, 1991.
(32) Salahub, D. R.; Fournier, R.; Mlynarski, P.; Papai, I.; St-Amant, A.; Ushio, J. In *Density Functional Methods in Chemistry*; Labanowski, J., Andzelm, J., Eds.; Springer: New York, 1991.
(33) Daul, C.; Goursot, A.; Salahub, D. R. In *Grid Methods in Atomic and Molecular Quantum Calculations*; Cerjan, C., Ed.; Nato ASI C142; 1993; Vol. 23.
(34) Kasai, P. H.; Hedaya, E.; Whipple, E. B. *J. Am. Chem. Soc.* **1969**, *91*, 4364.
(35) Kasai, P. H.; Amer, J. *J. Am. Chem. Soc.* **1972**, *94*, 5950.
(36) Kasai, P. H.; Jones, P. M. *J. Am. Chem. Soc.* **1985**, *107*, 813.
(37) Kurtz, H. A.; Jordan, D. J. *J. Am. Chem. Soc.* **1980**, *102*, 1178.
(38) Sakai, S.; Jordan, K. D. *Chem. Phys. Lett.* **1986**, *130*, 103.
(39) Gonzalez, C.; Schlegel, H. B. *J. Chem. Phys.* **1989**, *90*, 2154.
(40) Gonzalez, C.; Schlegel, H. B. *J. Phys. Chem.* **1990**, *94*, 5523.
(41) Boys, S. F.; Bernardi, F. *Mol. Phys.* **1970**, *19*, 553.
(42) Howard, J. A.; Joly, H. A.; Edwards, P. P.; Singer, R. J.; Logan, D. E. *J. Am. Chem. Soc.* **1992**, *114*, 474.
(43) Basch, H.; Hoz, S. *J. Phys. Chem. A* **1997**, *101*, 4416.
(44) Durant, J. L. *Chem. Phys. Lett.* **1996**, *256*, 595.
(45) Fängström, T.; Eriksson, L. A.; Lunell, S. *J. Phys. Chem. A* **1997**, *101*, 4814.